sciendo
Power Electronics and Drives
Volume 9(44), 2024 DOI: 10.2478/pead-2024-0019



# An Experimental Set-up Involving Low-cost Digital Controller to Study the Magnetizing Inrush Current in a Transformer using Point-on-Wave Switching Technique

**Research paper**

Ananya Nayak, Dipankar Chatterjee*, Suvarun Dalapati

*Electrical Engineering Department, Indian Institute of Engineering Science and Technology, Shibpur, Howrah, India*

**Received: 31 December 2023; Accepted: 02 April 2024**

**Abstract:** Generally in under-graduate studies, magnetizing inrush current (MIC) is discussed theoretically without giving much practical exposure. This paper presents the development of a low cost experimental set-up using a digital controller to study the MIC and the different parameters which can affect the same. This also helps to show how the inrush current can be minimized. This set-up also provides a hands-on experience of MIC and its control in under-graduate study, which can help an upcoming practitioner in industry as well as in further research. This paper presents a brief description of MIC, followed by a short analysis. Here, a pair of anti-parallel thyristors are connected in series with the primary winding of a single-phase power transformer. The turningon instant of this switch, with respect to the zero-crossing instant of the input supply voltage, may be adjusted through a firmware, in a PIC18F4620 from Microchip Technology microcontroller development board from Microchip Technology to control the transformer energisation instant. The firmware is developed in MPLABX-IDE from Microchip Technology, and the scheme is verified via simulations in Proteus simulation software. A suitable circuit to support the microcontroller development board to achieve the above function is designed and fabricated.

**Keywords:** *microcontroller • point on wave switching technique • zero-crossing detector • thyristor • transformer magnetizing current*

## 1. Introduction

One of the most important abnormalities inside transformer circuits is transients. These may be classified as internal and external transients. External transients are due to switching operations. Internal transients are mainly of three types: over excitation, internal fault, and magnetizing inrush current (MIC) (Wani et al., 2012). MIC is an unwanted phenomenon in transformers, due to which a transformer, when energized, draws a large amount of magnetizing current that is rich in harmonics and lasts for several cycles. Large inrush currents are caused when a transformer is initially connected to an AC voltage source (Blume et al., 1944), and they are encountered even when the transformer is energized at no-load condition. Such inrush currents may reach huge peak levels at the start (about 30 times the value of rated winding current), decay significantly under tenths of a second, while its complete decay could takes seconds. The waveform of a typical inrush current displays DC offsets and sometimes even harmonics of varying magnitudes, often comprising of second and other even harmonics. Figure 1 represents the MIC in a typical case when the core is highly saturated. This clearly includes the non-linear behaviour of the core material in its highly saturated zone. The current has a large DC component, and due to saturation, its profile deviates much from its sinusoidal nature, and it takes several cycles to decay to its steady-state value. Through experience, it can be inferred that this inrush current problem can be improved with advances in the art of transformer design and manufacturing.

* Email: dipankar.rs2018@ee.iiests.ac.in

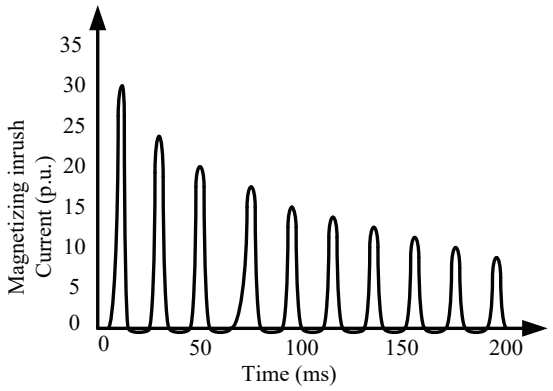


**Figure 1.** Magnetizing inrush current profile of a transformer with a highly saturated core.

The magnitude and the number of cycles in transients are determined by the following factors (Al-Khalifah and El Saadany, 2006; Blume et al., 1944; Jamali et al., 2011; Negara et al., 2017; Taylor et al., 2012):

- The instantaneous value of the supply voltage when the switch (connecting the primary winding with the supply) is closed.
- The magnitude and sign of residual magnetism, present in the core, with reference to the very first half cycle of the alternating flux, as set up by the connected voltage supply.
- Magnetic property of the core material, particularly the maximum flux-carrying capacity of the core.
- The magnitude of the inrush current depends upon the impedance value, and its damping depends upon the total resistance in primary winding from the equivalent source.
- In general, for increased current rating, the expected peak value of inrush current also increases.
- Physical arrangement of the excitation winding.

Some of the major problems caused by the inrush current are voltage sag and distortion at the receiving end of the line where the transformer is connected, spurious tripping of over-current relays, system resonance due to significant number of harmonics in inrush current, additional power losses in the form of heating and core losses, oscillating torques in the motor leading to increased vibration, mechanical stress on the motor components etc. Repeated occurrence of inrush currents during frequent starts and stops can accelerate the wear and tear of motor components, including bearings, windings, and rotor laminations. This can lead to motor deterioration and reduced reliability over time. Due to the above issues, it is crucial to analyse the transformer MIC in detail.

Intensive research is ongoing for analysing the MIC in a transformer, which has led to the development of newer techniques for reducing its magnitude as well as its effect on the system. (Naseri et al., 2018) present a technique for discriminating the MIC from the internal fault current. The non-linear state-space model for a single-phase transformer is developed. Thereafter, an extended Kalman filter (EKF) is utilized for estimating the primary winding current; however, the EKF is not effective in estimating the current in case of a fault in a transformer, because of the large model mismatches. For modeling the transformer magnetization curve, this technique is directly dependent on transformer data. In the study by Batista et al. (2018), the transformer MIC is distinguished from a fault current. Here, generalized delayed signal cancelation (GDSC) is used to compute the fundamental and second-harmonic positive and negative sequence components and to create a possible distinction by analysis of less number of samples. However, this technique suffers from high computational burden and complexity, redundant representation in the time–frequency space etc. Hooshyar et al. (2012) present a power-based algorithm for discriminating between internal faults and switching conditions of transformers. Here, the differential power signal is analysed by introducing its intrinsic features in inrush conditions. Thereafter, using these features, a combined wave-shape classification technique in the time-domain is proposed, resulting in two discriminative indices. These indices can help identify the inrush power signals within half a cycle. The technique though remains unaffected by power system parameters, transformer magnetizing curves, operating conditions etc., but the white Gaussian noise can distort the current and voltage time series. Bi et al. (2007) present an algorithm based on the waveform correlation analysis

for distinguishing between the short-circuit fault current and the MIC. This method uses the differential current waveform characteristics in the non-saturation zone. The non-saturation zone is first decided by comparing the algebraic sum of sampling data within a short slide window of the differential current and thereafter, the two kinds of normal sinusoidal waveforms are structured according to the value of differential current in the non-saturation zone. The magnetizing inrush and internal fault conditions are identified in the work of He et al. (2006) through an error estimation-based technique. Here, the actual wave is compared with two reference waves within a half cycle for two different frequency conditions. The technique may fail in timely responding to the fault, resulting in blocking the zero-sequence current protection of the upstream line.

The differential current has been processed by Faiz and Lotfi-Fard (2006) by considering different behaviours of the differential currents under inrush current and fault conditions. Here, a criterion function using the wavelet coefficient amplitude difference within a specific frequency band is utilized for discriminating internal faults from inrush current within a quarter cycle after the disturbance. However, this technique, based on wavelet, does not provide satisfactory classification accuracy rate. A technique to detect internal faults during inrush conditions has been proposed in Medeiros and Costa (2018), where the differential protection principle is applied using the operating and restraining wavelet coefficient energy. This technique does not require harmonic information. The proposed differential technique has been evaluated for sympathetic inrush condition, different transformer energisation in different conditions, etc. Transformer T and $\pi$ models, derived in León et al. (2012), show same steady state accuracy, but better accuracy in calculating the inrush currents in the case of the $\pi$-equivalent circuit. The model, having two magnetizing branches, has more degrees of freedom in developing the dual, reversible transformer model. Jazebi et al. (2015) presents an accurate analytical technique for computing the maximum inrush currents, which estimates the inrush currents with high precision, considering different hysteretic shapes. This involves simple steps for solving the linear governing differential equations. The inrush currents can be reduced by increasing the resistance or saturation inductance, but the transformer becomes less efficient with increase in resistance. During approximation of the magnetizing characteristics, the identification of the proper saturation level is difficult. The effect of the MIC on power quality of common connection points can reflect the degree of influence of all transient processes in the traction power supply system on the power grid quality. In Sobrinho et al. (2016), the total loss optimization technique-based, single-phase distribution transformer design has been proposed, where particle swarm and differential evolution are the techniques used. In Hamilton (2013), a simplified excitation curve, based on the saturation flux and residual flux, is developed for analyzing the MIC during transformer energization. However, for inrush current having low harmonic content, high reliability but low security can be achieved by the harmonic restraint algorithm. This may also provide an unexpected blocking during energisation of a faulty transformer having high harmonics in healthy phases. More destructive currents can be drawn by the transformers as compared to inrush currents, in case residual flux exists in the cores or when the ‘phase-hop’ phenomenon occurs (Farazmand et al., 2014). In a power system, phase-hop phenomenon can occur at any time due to voltage sags, interruptions, or notching in the network, which cannot be predicted. The phase-hop current may have twice the magnitude as compared to the zero-crossing inrush currents.

Continuous research is going on in this area, which involves development of different techniques, for more intense analysis and for reduction of MIC. Some of the recent works are discussed in the following. Chen et al. (2023) proposed an asynchronous, closing technology-based strategy for eliminating the MIC for hybrid transformers (HTs). Here, the parallel auxiliary winding (PAW) for the HT is developed and utilized for establishing a step-type, synchronous magnetic field having residual magnetism. The stabilisation time of the primary voltage signal and oblique wave of the grid are controlled and the non-synchronous closing of the HT mitigates the MIC generation. Pachore et al. (2021) proposes an inrush current minimisation technique for a 3-phase transformer through a controlled switching strategy, which involves a gang-operated circuit breaker. The residual and prospective fluxes help in calculating the flux error function for obtaining the optimum points for controlled closing and opening of the switch. The flux transient behaviour, mechanical closing time variation and voltage error measurement have also been discussed. In Jin et al. (2020), a modified time difference technique is proposed to remove the maloperation of the zero-sequence overcurrent protection for the upstream transmission line due to high MIC in a high-voltage, built-in high-impedance transformer (HVBHT). Here, the substation area information is utilised for accurate identification of the MIC.

Wang et al. (2023) proposes a wavelet transform-based technique to identify the MIC and fault current. The current signal results are anyalsed through wavelet transforms. This technique can effectively identify the difference

between the inrush current and the fault current. Yahiou et al. (2022) present the influence of the inrush current on the hysteresis loop of a single-phase transformer, in terms of its position, area and size. A particle swarm algorithm-based optimized support vector machine (SVM) MIC recognition model has been presented in Duan et al. (2022). The MIC and internal faults are identified through feature extraction of the current waveform. In Moreira et al. (2021), a directional gradient technique-based algorithm is proposed for distinguishing the inrush currents from the source surge current or fault currents in transformers. The effectiveness of the gradient technique has been analysed for the situations of false operation of the protection systems. In Liu et al. (2021), a technique for MIC identification has been proposed, which involves the empirical mode decomposition index and artificial intelligence algorithm. The energy index for each inherent model component is obtained and thereafter simplified using the mean impact value technique.

Thus, from the above discussion, it can be stated that the inrush current phenomenon has been widely analysed, and different techniques have been proposed to reduce its occurrence. The present manuscript has been written from a completely different point of view. Generally in under-graduate studies, theoretical discussion is included regarding MIC without giving much practical exposure. This paper actually presents the development of a lowcost experimental set-up using a digital controller to study the MIC phenomenon and the different parameters which can affect the same. This also helps in showing how the inrush current can be minimised. This set-up provide a direct hands-on experience regarding MIC and its control in under-graduate study, which can help an upcoming practitioner in industry, as well as in further research. By using the proposed experimental set-up, various effects related to the MIC can be studied. These effects include the amplitude and duration of the inrush current, along with the influence of different transformer parameters, its impact on the transformer and associated equipment, and the effectiveness of protective measures to mitigate the problem. The set-up will enable controlled experiments, and data collection and comprehensive analysis of the inrush current phenomenon.

## 2. Magnetizing Inrush Current Phenomenon: A Brief Discussion

Let supply voltage $v = V_m \sin \omega t$

$e$ = emf induced in primary winding

$N$ = No. of turns of primary winding

For an ideal transformer, $v = e$ as it is an ideal transformer, neglecting core loss and resistance of primary winding.

Thus, the magnetic flux can be expressed as

$$\varphi = \frac{1}{N}\int v dt$$

$$= \frac{V_m}{N\omega}\sin\left(\omega t - \frac{\pi}{2}\right) \tag{1}$$

The current waveform is in the same phase with the flux waveform and 90° behind the voltage waveform, provided that the core is working in the linear region of the B-H curve. Depending on the instant at which the winding is connected to the supply, the core may saturate and hence, may not operate in the linear zone. If the transformer is switched on at the instant of zero-input voltage, the inrush current will have maximum value. Similarly, if the transformer is switched on at the instant when the value of the input voltage is close to its positive or negative amplitude, the inrush current will have its minimum value. However, this demands that the transformer primary winding to be connected to the supply at a specific instant, which is difficult to achieve in practice, particularly if the transformer is operated manually. This is actually referred to as the pointonwave switching technique.

However, a difference exists between the sudden starting mode and continuous mode of operation. When switched on to the supply voltage, the flux in the transformer core is generally at its residual levels, which is a small percentage of the flux, which the core can support. Thus, when connected to the supply, the magnetic flux will increase from nearly zero, and not from any arbitrary magnitude. This directly implies that the nature and peak value of the flux in the core depends on the instant at which the exciting winding is connected to the supply voltage. One

extreme case is mentioned here when the transformer core has zero residual flux and is switched on to the supply voltage at the instant of its positive zero-crossing. For such a case,

$$\varphi = \varphi_m + \varphi_m \sin\left(\omega t - \frac{\pi}{2}\right), \tag{2}$$

where $\varphi_m$ is the maximum value of the flux in steady state.

Now, it can be observed that the maximum value of the flux waveform is $\phi = 2\varphi_m$, i.e. the resultant flux will reach at maximum value of $2\varphi_m$ at the instant of switching at zero value of supply voltage. This is known as doubling effect. Generally, the residual flux value is a small percentage of the rated flux, and Eq. (2) is approximately valid even in presence of residual flux. As the core is generally designed to operate near the knee-point of the B-H curve under normal rated conditions, such a flux-equation implies that the core is certain to saturate within the first half cycle of the flux wave. Since this implies that the core will go deep into the saturation zone of the BH curve, a large magnetizing current is bound to be drawn from the supply under such situation. In case the residual flux is a large percentage of the rated flux and the magnetization produces flux in the same direction (from the supply voltage), then the core will reach saturation more quickly and the case will be more severe. The resultant flux will now go to maximum value $(2\varphi_m + \varphi_{res})$, where $\varphi_{res}$ is the residual flux. The core now goes into the deep saturation region of magnetization, as shown in Figure 2 and the corresponding value of the magnetizing current will have a very high peak value.

As the core can carry only a finite amount of flux, all of this large amount of flux may not be carried by the core. The excess amount of flux flows through the air (or free space) surrounding the core. The flux which is carried out by the free space is given by

$$2\varphi_m + \varphi_{res} - \varphi_{sat} = \varphi_1. \tag{3}$$

The current which produces this flux in free space (Blume et al., 1944) is

$$I_{mex} = \frac{\varphi_1}{L_1}. \tag{4}$$

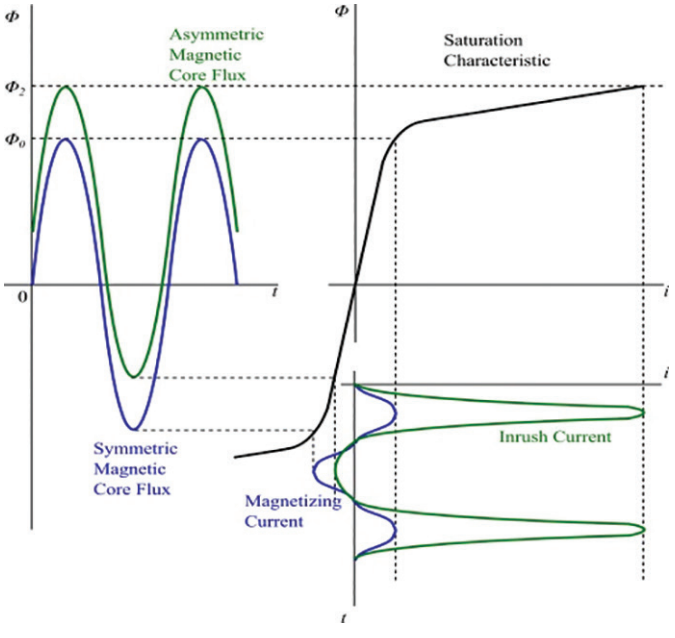


**Figure 2.** Graphical representation of the inrush current phenomenon (Al-Khalifah and El Saadany, 2006).

When dealing with very high flux densities in a transformer, it becomes a challenge to obtain the hysteresis loop. At such high flux densities, the core material may exhibit non-linear magnetic behaviour and may reach at saturation. Due to the difficulty in obtaining hysteresis loop data at these extreme flux densities, estimating the corresponding current wave becomes more complex. So, with close approximations, simplified models can be developed to calculate the values of current. However, the actual behaviour of the inrush current can vary based on factors such as core saturation effects, core materials, winding configuration, and the specific conditions during energisation.

A simplified formula which is often used to estimate the peak value of the inrush current for saturated range air core inductance of solenoidal winding of a single-phase transformer (Blume et al., 1944) is

$$I_m = \frac{1000\ hB_s}{3.2n}, \tag{5}$$

where $B_s = \frac{A_c}{A_s}\left(2B_m + B_{res} - B_{sat}\right)$.

Here, $A_s$ = area occupied by the core legs, plus the space between the core legs and the excited winding.

$A_c$ = cross-sectional area of the core

$B_m$ = maximum flux density of core

$B_{res}$ = residual flux density of core

$B_{sat}$ = maximum flux density of iron molecules

$h$ = length of the solenoid

$n$ = Number of turns in series

The first part of Eq. (5), $\frac{A_c}{A_s}$, represents the ratio of the cross-sectional areas of the core to the winding. This ratio helps to determine the impact of the core on the magnetic field. The second part of Eq. (5), $\left(2B_m + B_{res} - B_{sat}\right)$, takes into account different magnetic properties of the core material. These values indicate the limits and characteristics of the core material's magnetic behaviour. By combining these factors, the equation provides an estimation of the peak magnetic flux density $B_s$ in the transformer core.

The large inrush current will decay quickly because of primary winding resistance. Now,

$$\Delta\varphi = \int_0^{\pi} Ridt, \tag{6}$$

where $\Delta\varphi$ signifies how much the core flux changes with time for each cycle of the inrush current, and $i$ is the magnetizing current. From this, it can be concluded that the inrush current immediately begins to decay, and this decay will continue till the magnetizing current of the transformer becomes symmetrical.

The magnetic flux can now be represented as

$$\varphi = (\varphi_{res} + \varphi_m cos\theta - \varphi_m \cos\left(\omega t + \theta\right)) - R\int_0^t idt, \tag{7}$$

where

$\varphi_{res}$ = residual flux at the instant of energising the transformer,

$\varphi_m$ = maximum flux value at steady state,

$R$ = resistance of the primary winding, where magnetizing current flows,

$\varphi$ = instantaneous flux at any time,

$\theta$ = phase angle measured from the zero instant of voltage to the instant of transformer energisation.

This inrush current has two components: a sinusoidal AC component and a DC component. Maximum peak inrush current is obtained at $\theta = 0, \pi, 2\pi, \ldots$. When the switching angle of the transformer is changed, it seems as though the peak of the inrush current of the first cycle is reduced. Core loss and eddy current loss may be factors influencing the rate of decay of inrush current. As eddy current loss depends on the current value, it may be partially influenced during the first few cycles, when the rate of decay is highest. There are several techniques for reducing MIC (Avinash, 2015; Basu and Asghar, 2008; Kumar and Reddy, 2014; Mirkalaei and Hashiesh, 2015; Taylor et al., 2012).

When the transformer is switched on and the supply voltage is impressed on the transformer terminals, there exists a DC-offset in the magnetic flux in the transformer core which causes MIC (Bimbhra, 2007; Blume et al., 1944). The DC-offset in the core flux and the inrush current depend on the point on the supply voltage where the transformer switching occurs. These attain their maximum values while switching at zero-crossing of the supply voltage and minimum values while switching at 90° position of the supply voltage. The magnitude and polarity of the residual flux also affects the core flux and the inrush current Thus, while the transformer goes through a magnetizing inrush, the magnetic flux becomes asymmetric with its increased peak value, and this has a direct impact on the transformer secondary voltage. Hence, the transformer secondary voltage also becomes asymmetric with its increased peak value. After a few cycles, this DC-offset becomes zero due to existence of resistance of the winding, and the core flux and magnetizing current become steady and symmetric, which make the secondary voltage steady and symmetric. Even during magnetizing inrush, the line resistance decreases the voltage supplied to the transformer terminals and makes it asymmetric, and there is a decrease in the core flux, which reduces the secondary voltage compared to what was expected without line resistance during inrush.

## 3. Initial Testing of Inrush Current of a Transformer

Figure 3 shows the experimental circuit diagram for measuring the inrush current of a single-phase transformer. To get a first-hand approximate idea regarding the magnitude of inrush current in the given test transformer (1 kVA, 50 Hz, 2:1 ratio, shell-type singlephase), the transformer has been energised repeatedly at arbitrary instants, and the readings on a moving iron- type (deflecting type) ammeter, connected in series with the primary winding, have been observed. In this initial experiment, the energisation of the transformer at different angular positions of the supply voltage can happen, as the transformer is connected to the supply voltage through a manually operated MCB. The peak deflection of the pointer of this ammeter gives an estimate of the value of the magnetizing current, as is displayed by the ammeter, and the time required for the pointer to settle gives us an idea regarding the time required for the current to settle. It may be noted that the peak value, as displayed by the deflecting-type ammeter, is not the actual peak value of the inrush current, as is drawn by the transformer in the first one or two half-cycles. It is so because the meter measures the fundamental-RMS value, and the time taken by this pointer to deflect to the peak position itself equals several full cycles of the current. Due to random switching i.e. connecting the transformer to the supply voltage at its different angular positions, results in different inrush current values as mentioned in Table 1. However, in each case, the steady state current remains the same. This is well applicable when the load is attached to the secondary side of the transformer. In such a case, due to addition of the load, the ammeter reading includes the effect of the secondary current on its primary side. As in this experiment, deflecting-type ammeter is used, thus the inertia of this measuring device directly affects i.e. increases the settling time. Despite the fact that the deflecting-type ammeter used in the initial experimental procedure cannot capture the MIC accurately, this exercise is carried out to give a first-hand approximate estimate of the magnitude of the inrush current and decay time, which may be used to select the fuses, relays, and circuit breakers and ammeters for the experimental set-up. The fuses are to be selected carefully in such a way that these are not only capable of withstanding the transformer inrush current, but also are not of unnecessarily large rating, which may result in inadequate protection

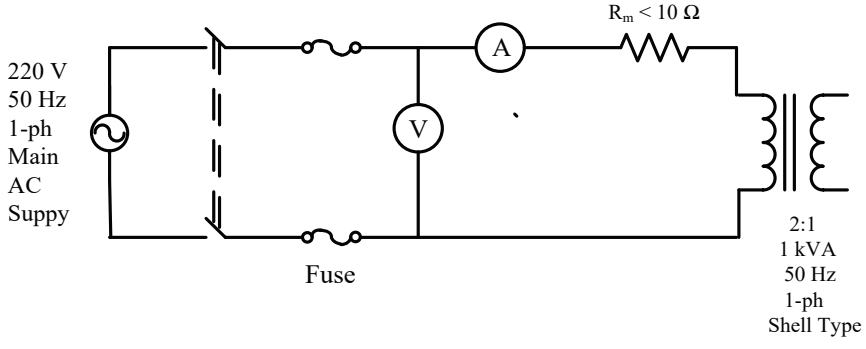


**Figure 3.** Circuit diagram for measuring the inrush current of a single-phase transformer.

of the transformer as well as the system. The percentage differential relays used to protect the unit in case of any internal fault may respond to transformer inrush current, as it flows in the transformer's primary winding only. Hence, the ammeter reading, which gives the approximate information regarding the inrush current, helps in determining the sensitivity as well as the response time of the relay. The ammeter reading also helps in selecting the rating of the circuit breaker in the same way as mentioned above, otherwise the circuit may trip, when the peak value of the inrush current in the initial cycles exceeds the current rating of the circuit breaker. The first-hand approximate estimate of the magnitude of the inrush current and decay time also provide primary information, based on which the solid-state switch ratings may be decided. Table 1 and Table 2 show that there is no appreciable change in the range of magnitude of the inrush current, with and without load. So, it is concluded that the load is not an influencing factor for the inrush current.

When an external resistance is connected with the primary winding of a transformer, the peak value of the primary winding current changes. To investigate this issue, an experiment has been performed, where it is required to energise a transformer at the same angular position of the supply voltage throughout the experiment. This can ensure a more accurate comparative analysis regarding the impact of inserting different values of external series resistance (on the primary side of the transformer) on the peak value of MIC. Here, again the experiment has been performed using a zero-crossing detector, which can detect the zero-crossing of the supply voltage, immediately energising the transformer through a relay. This ensures near zero point switching of the transformer, considering the uniform delay in relay operation for each of the readings. In Table 3, it is observed that if the resistance is increased, then the peak value of primary current decreases.

Using a series resistance may be allowed only during the transient magnetizing period, and not for the steady state operation, as it will invariably result in ohmic losses and reduced effective primary voltage, causing unacceptable regulation in overall efficiency during steady state of operation. It is also to be mentioned that the considerable inertia of the deflecting type ammeter prevents the precise determination of the settling time of the

**Table 1.** Measuring inrush current with no load.

| Sl. No. | Voltmeter reading (V) | Ammeter reading (A) | | Time to settle (s) |
|---|---|---|---|---|
| | | Peak point deflection | Steady state | |
| 1 | 218 | 12 | 2.6 | 1.97 |
| 2 | 218 | 13 | 2.6 | 2.40 |
| 3 | 218 | 10 | 2.6 | 1.78 |
| 4 | 218 | 10.8 | 2.6 | 1.79 |
| 5 | 218 | 8 | 2.6 | 1.66 |
| 6 | 218 | 10 | 2.6 | 1.88 |
| 7 | 218 | 14 | 2.6 | 2.58 |
| 8 | 218 | 8.4 | 2.6 | 1.56 |
| 9 | 218 | 10 | 2.6 | 1.78 |
| 10 | 218 | 13.8 | 2.6 | 2.48 |

**Table 2.** Measuring inrush current with load.

| Sl. No. | Voltmeter reading (V) | Ammeter reading (A) | | Time to settle (s) |
|---|---|---|---|---|
| | | Peak point deflection | Steady state | |
| 1 | 218 | 8.4 | 3.4 | 2.08 |
| 2 | 218 | 12.4 | 3.4 | 2.30 |
| 3 | 218 | 12 | 3.4 | 2.37 |
| 4 | 218 | 4.8 | 3.4 | 1.35 |
| 5 | 218 | 8 | 3.4 | 2.12 |
| 6 | 221 | 7.8 | 3.6 | 2.23 |
| 7 | 218 | 4.8 | 3.4 | 1.11 |
| 8 | 218 | 14 | 3.4 | 2.31 |
| 9 | 218 | 6 | 3.4 | 2.03 |
| 10 | 218 | 8.4 | 3.4 | 2.11 |

**Table 3.** Measuring inrush current, with external resistance connected in series with the primary side winding of the transformer.

| Sl. No. | Primary side external resistance (Ω) | Voltmeter reading (V) | Ammeter reading (A) | | Time to settle (s) |
|---|---|---|---|---|---|
| | | | Peak point deflection | Steady state | |
| 1 | 4 | 220 | 6.5 | 2.7 | 1.75 |
| 2 | | 220 | 6.5 | 2.7 | 1.75 |
| 3 | | 220 | 6.7 | 2.8 | 1.71 |
| 4 | | 221 | 6.7 | 2.7 | 1.81 |
| 5 | | 221 | 6.8 | 2.8 | 1.73 |
| 6 | 3 | 220 | 9.9 | 2.8 | 1.82 |
| 7 | | 219 | 9.5 | 2.7 | 1.85 |
| 8 | | 219 | 9.8 | 2.8 | 1.85 |
| 9 | | 220 | 9.8 | 2.8 | 1.88 |
| 10 | | 221 | 9.9 | 2.7 | 1.82 |
| 11 | 2 | 221 | 12.1 | 2.7 | 1.89 |
| 12 | | 220 | 12.4 | 2.6 | 1.91 |
| 13 | | 219 | 11.9 | 2.7 | 1.93 |
| 14 | | 220 | 12.7 | 2.6 | 1.96 |
| 15 | | 220 | 12.1 | 2.6 | 1.94 |
| 16 | 1 | 221 | 22.1 | 2.6 | 2.04 |
| 17 | | 221 | 22.1 | 2.6 | 2.01 |
| 18 | | 220 | 22.4 | 2.7 | 1.98 |
| 19 | | 219 | 22.6 | 2.6 | 2.06 |
| 20 | | 219 | 22.6 | 2.6 | 2.01 |

**Table 4.** Measuring inrush current with no load and values taken from DSO.

| Sl. No. | Voltmeter reading (V) | DSO reading (A) | | Time to settle (ms) |
|---|---|---|---|---|
| | | Peak point deflection | Steady state | |
| 1 | 220 | 28.8 | 2.8 | 240 |
| 2 | 220 | 32.8 | 2.8 | 240 |
| 3 | 220 | 23.6 | 2.8 | 220 |
| 4 | 220 | 46.8 | 2.8 | 280 |
| 5 | 220 | 18 | 2.8 | 300 |
| 6 | 220 | 34 | 2.8 | 280 |
| 7 | 220 | 24 | 2.8 | 260 |
| 8 | 220 | 36 | 2.8 | 240 |
| 9 | 220 | 32 | 2.8 | 280 |
| 10 | 220 | 23.5 | 2.8 | 220 |

DSO, digital storage oscilloscope.

ammeter to its steady state. The damping co-efficient of the deflecting-type ammeter has a direct impact on settling time of the deflecting- type ammeter. As a result, it takes more time to settle to its steady state, which is reflected in the column 'Time to settle' of Tables 1–3. Thus, it provides an approximate idea regarding the trend of the settling time, not the accurate one.

For further verification, the inrush current is measured by a digital storage oscilloscope (DSO). For measuring this current, a small resistance is connected in series with the primary winding of the transformer, and the current is measured as a voltage drop across that resistor. The experimental data are presented in Table 4, and the current waveform is shown in Figure 4. Compared to Table 1, the settling time of the inrush current is significantly reduced in Table 4 due to the addition of a resistor for current measurement. However, the waveform still exhibits a dip, caused by the presence of inrush current for several cycles. Figure 4 displays the first few cycles of the inrush current captured by the DSO. These initial cycles exhibit a combination of the dc-offset and some even harmonics in the current waveform.

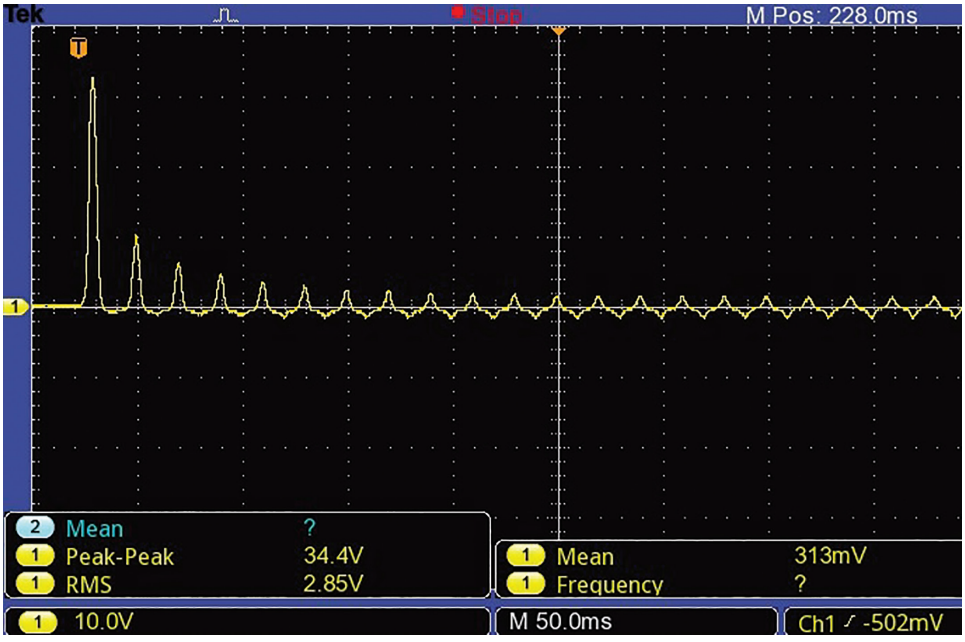


**Figure 4.** Photography of waveform of inrush current of 1-ph 1 kVA transformer taken by DSO. Scales: X-axis: 50 ms/div Y-axis: 10 A/div. DSO, digital storage oscilloscope.

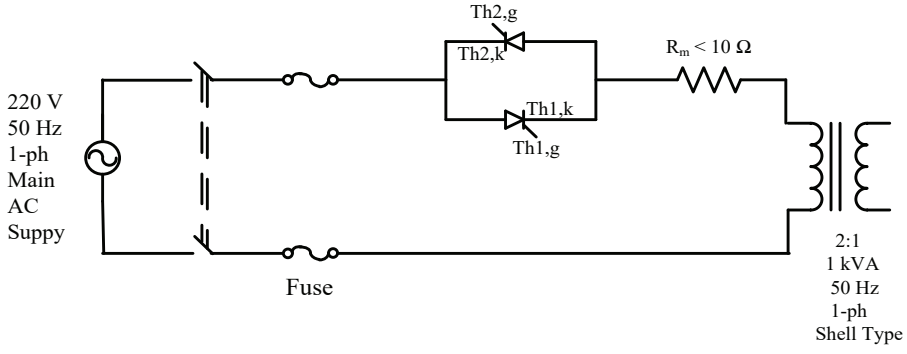


**Figure 5.** Circuit diagram of the measuring inrush current of a transformer, which is controlled by a thyristor switch.

# 4. Hardware Set-up to Observe Inrush Current with Controlled Switching Instant

In the experimental set-up shown in Figure 5, two anti-parallel 400 V, 25 A SCR switches are used. Here, a 1 kVA, 220 V transformer is used, i.e. 4.5 A rated current flows through primary winding of the transformer while delivering the rated load. Here, a Vishay, 25TTS12- type thyristor has been selected, which has a current rating of 25 A and a voltage rating of 1,200 V. In Figure 5, the switching time of the thyristor can be controlled by applying the gate pulse at a desired instant after the zero-crossing of the supply voltage.

## 4.1. Proposed control circuit diagram for experimental set-up

Figure 6 shows the block diagram of triggering of the thyristor switch. The purpose of the control circuit design for a thyristor is to provide precise control over the gate triggering signal of the thyristor. The desired control circuit employs various components, such as the zero-crossing detector, a microcontroller, a signal amplifier, a driver circuit, and an isolation circuit. The zero-crossing detector synchronizes the thyristor's operation with the AC supply voltage, and it provides a signal to the microcontroller, which determines the desired timing and delay for triggering the thyristor, based on the target switching operation. The microcontroller generates a control signal, which is

amplified by the signal amplifier to the necessary voltage and current levels required for the driver circuit of a thyristor. The amplified control signal is then fed into the driver circuit, which provides the necessary gate voltage and current pulses to trigger the thyristor. Additionally, an isolation circuit is integrated to offer galvanic isolation and safeguard to the control circuitry from electrical noise, voltage spikes, and other potential hazards.

Firstly, the on-card power supplies for powering up the various electronic components on the cards, are designed. In the whole set-up in Figure 6, the micro-controller is energised from 5 V DC, and other components are energised from 15 V DC. These power supplies are set up by using step-down transformers, which operate directly from 220 V, 50 Hz AC lines. The zero crossing detector (ZCD) detects the zero crossing of the supply voltage, and the diode on the output pin of the OP-AMP ensures that the negative half of the pulse does not reach the micro-controller input pin. As output of ZCD is 15 V, a voltage-divider circuit is required so that the input signal of the micro-controller is less than 5 V. The micro-controller is to be programmed in such a way that the triggering instant, with respect to the zero-crossing of the supply voltage, may be selected by the user via a potentiometer so that switches turn on accordingly. As a 15 V supply is required for the driver circuit, a signal amplification stage is also required. After the driver circuit, the gate signal for both thyristor switches may also be obtained (Mohan et al., 2003).

Figure 7 shows the circuit diagram of the set-up of the driver circuit for triggering SCR. ZCD detects the zero crossover on the voltage wave. It distinguishes between the starting points of the positive half cycle and negative half cycle. The 220 V AC voltage is stepped down by a transformer and delivers secondary output of 5 V, 100 mA. This voltage is converted into a ±15 V AC square wave by ZCD. A 1N4007-type diode converts the ±15 V square wave to a +15 V DC square wave and thereafter into a +5 V DC square wave by the voltage divider circuit. The 'potential divider' block has the function of reducing the ZCD output voltage suitably to ensure that the final output, reaching the microcontroller, is within the tolerable limits of the microcontroller pin. As the microcontroller input should be within 0–5 V, so zener diode of 4.7 V rating is used to make the output voltage of ZCD within

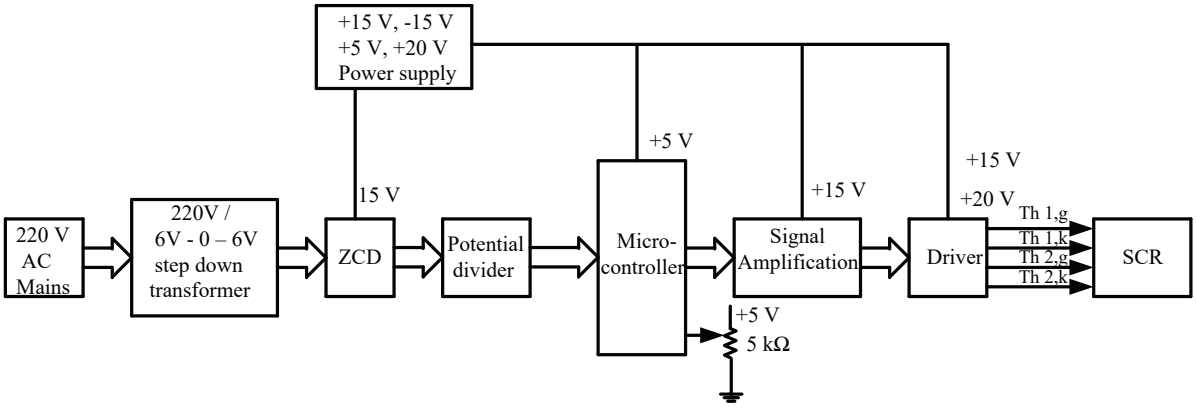


**Figure 6.** Block diagram of the triggering scheme of a thyristor switch. ZCD, zero crossing detector.

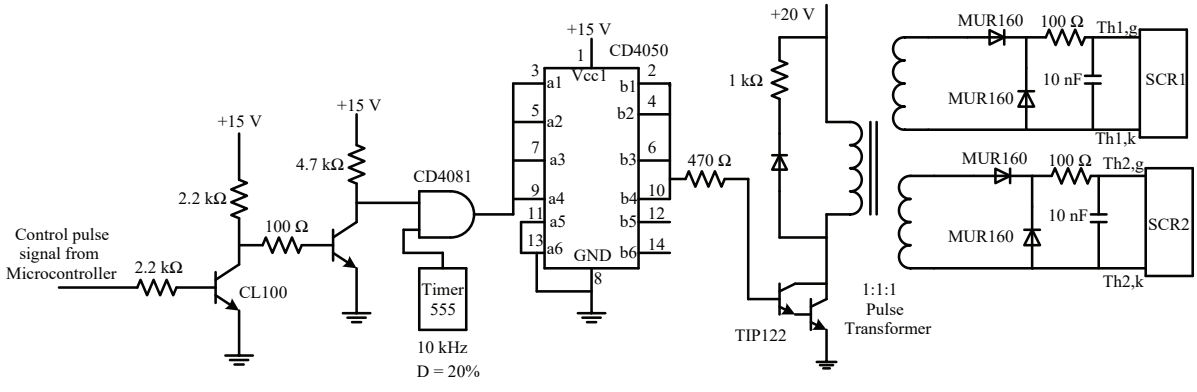


**Figure 7.** Circuit diagram of the experimental set-up of a driver circuit for triggering SCR.

**Table 5.** Analog input voltage and corresponding firing angle.

| Sl. No. | Analog input voltage (V) | Corresponding angle (°) |
|---|---|---|
| 1 | 0 | 0 |
| 2 | 0.5 | 18 |
| 3 | 1 | 36 |
| 4 | 1.5 | 54 |
| 5 | 2 | 72 |
| 6 | 2.5 | 90 |

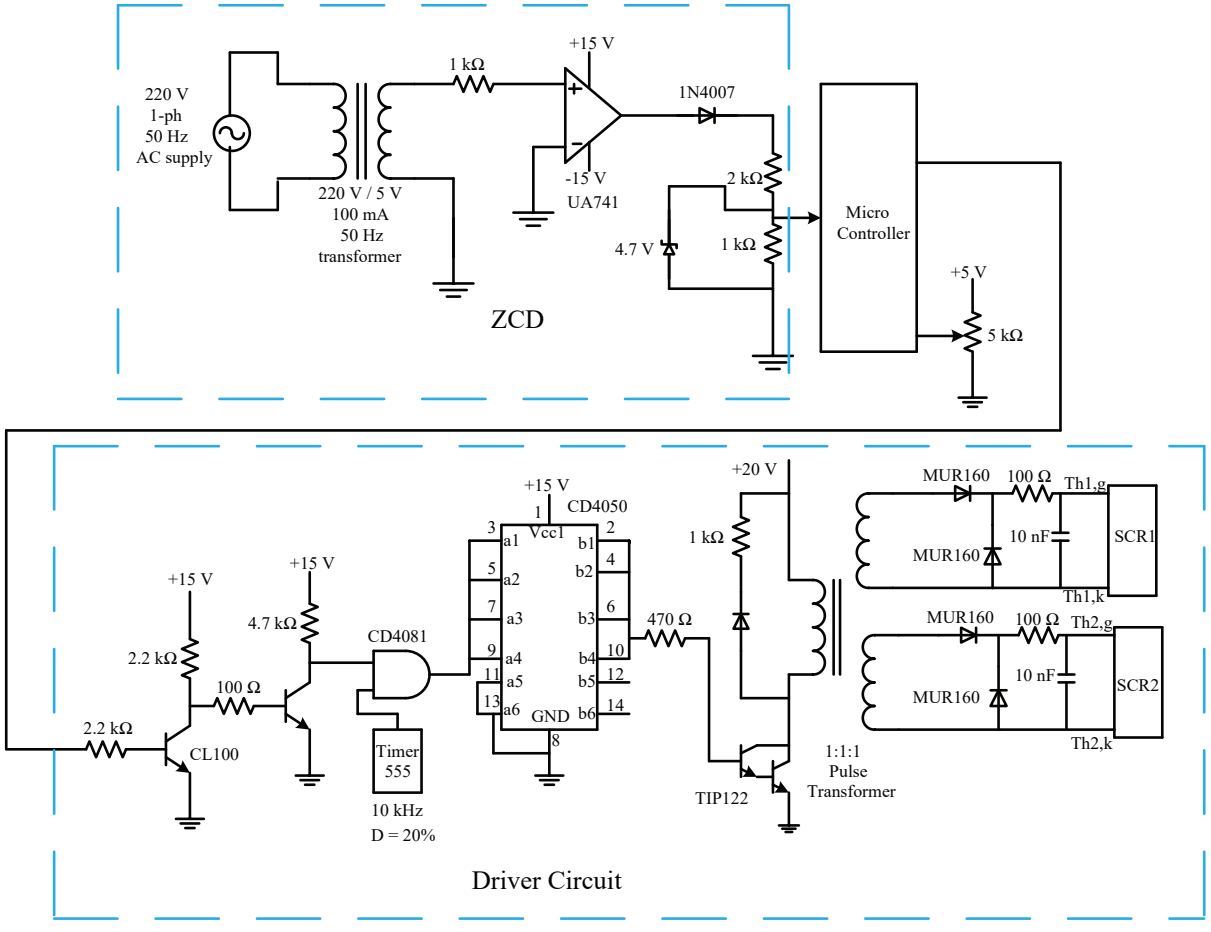


**Figure 8.** Circuit diagram of experimental set-up of complete control circuit for triggering SCR. ZCD, zero crossing detector.

4.7 V. The 5 kΩ potentiometer feeds a variable analog DC voltage to an ADC input pin of the microcontroller. This potentiometer is available to the user and, hence, the analog voltage, reaching the microcontroller, can be adjusted by the user. This analog voltage sets the delay angle, measured from the zero-crossing of the input voltage at which the solid-state switches will be triggered, thereby connecting the transformer primary-winding to the input AC supply (Figure 5). Thus, this 5 kΩ resistor helps the user to set the triggering angle value. Table 5 has been provided to the user, which will state the value of the triggering angles for various output voltage values derived using the 5 kΩ potentiometer. Signal amplification is done by two CL100-type BJT, connected back-to-back.

The complete control circuit for triggering the SCR is shown in Figure 8. The control signal is modulated by high-frequency pulses before the driver circuit of the thyristors because high-frequency switching reduces the size of the pulse transformer and gate power dissipation of the solid-state devices. For a high-frequency signal, 555-Timer of 10 KHz and 20% duty cycle is used. However, higher frequencies may also introduce additional switching losses

and electromagnetic interference (EMI). Also, duty cycle is a compromise between reducing the inrush current and minimising the unwanted harmonics. So, a 10 kHz frequency and 20% duty cycle strikes a reasonable balance between these factors. To combine these two signals, a CD4081-type AND GATE is used, so that the control signal has high-frequency pulses. After that, a CD4050-type buffer IC is used, which acts as a non-inverting, current boosting interface. TIP122 is an NPN, silicon power, Darlington pair, which is a super alpha circuit. As a control signal has a high frequency, a fast-response transistor is required.

It is necessary to have isolation in the driver circuit for safety reasons, for which a 1:1:1 pulse transformer is used. When the gate pulse of TIP122 is off, it means the transistor is turned off, and at that time, the diode starts to work. Subsequently, the diode allows the flow of current through the transformer. Here, both the diode and resistor work as a turn-off snubber circuit.

## 4.2. Operating area of experimental set-up

It is important to ensure that the inrush current experimental set-up can handle the transformer's rated power and operate at a 50 Hz frequency. Considering the worst-case scenario for inrush current, it is advisable to select a thyristor with a voltage rating of 400 V and a current rating of 25 A. However, a Vishay, 25TTS12-type thyristor has been chosen, which has a voltage rating of 1,200 V and a current rating of 25 A. The thyristor's high voltage rating of 1,200 V enables it to handle voltage spikes and surges during switching operations, ensuring reliable operation within its specified range. With a current rating of 25 A, the thyristor can handle continuous current up to 25 A without any issues. Additionally, it has a surge current rating of 300 A, indicating its ability to handle high-current spikes of short duration. It is essential to consider both the magnitude and duration of the inrush current in the system to ensure it to remain within the operating limits of the thyristor.

## 4.3. Micro-controller program and its validation

Now-a-days the switching technology of an analog triggering circuit is replaced by a digital triggering circuit. The analog triggering circuit is very complicated because of many components, and chances of noise in the signal are increased in the analog triggering circuit. In this work, a low-cost digital controller, PIC18F4620, is used, and the main objective of the microcontroller is delaying of firing angle of the thyristor. The digital triggering circuit overcomes the limitations of the analog triggering circuit such as shifting phase inaccuracies, debugging difficulties, and noise in the signal.

### *4.3.1. Proposed flowchart*

The flow chart of the proposed algorithm for a PIC18F4620 microcontroller is shown in Figure 9. Firstly, the microcontroller pins are configured. The RB0 pin is used for checking the voltage level of the ZCD output. For better result, the output of the microcontroller is withheld for some cycles. Delay in the firing gate pulse of the SCR switch is given for first one cycle, which is decided by setting the voltage level of the potentiometer detected by the RA0 pin. The analog value of the potentiometer is converted into its digital equivalent by the ADC available in the controller. TheTIMER register value is set as the digital value of the ADC. PIC18F4620 has a 10-bit ADC, but an 8-bit ADC is used in this program.

For adjusting the firing angle, the potentiometer is used, whose voltage can vary within 0–5 V. The pin RA0 of port A is used for A/D converter, and the analog voltage (0–5 V) is converted into (0–255) count accordingly. When the analog input value changes, the correspondingly digital count also changes in the microcontroller. Accordingly, the digital count delay of the triggering gate pulse of SCR is calculated. Here, crystal frequency is 10 MHz and pre-scalar value is 1:2, and each instruction cycle contains four machine cycles. Delay is given to firing the angle of SCR for one cycle. Here, the output of the micro-controller becomes same as the output of ZCD. The output of the micro-controller is injected into the gate driver circuit of the SCR switch.

### *4.3.2. Validation of proposed methodology by using Proteus software*

Here, the programme code implemented in PIC18F4620 is first verified in Proteus 8 software. Figure 10 shows the circuit diagram of the ZCD and microcontroller in Proteus, and the results are shown in Figure 11. The ZCD signal is connected to the RB0 of the microcontroller, and the output of the microcontroller is connected to RB1, and for calculation of delay angle, the potentiometer is connected to RA0. To analyse the waveforms, the ZCD signal and the output waveform can be observed at different points using an oscilloscope. Ch.A shows a 5 V, 50 Hz AC power supply, Ch.B shows the output of the OP-AMP used in

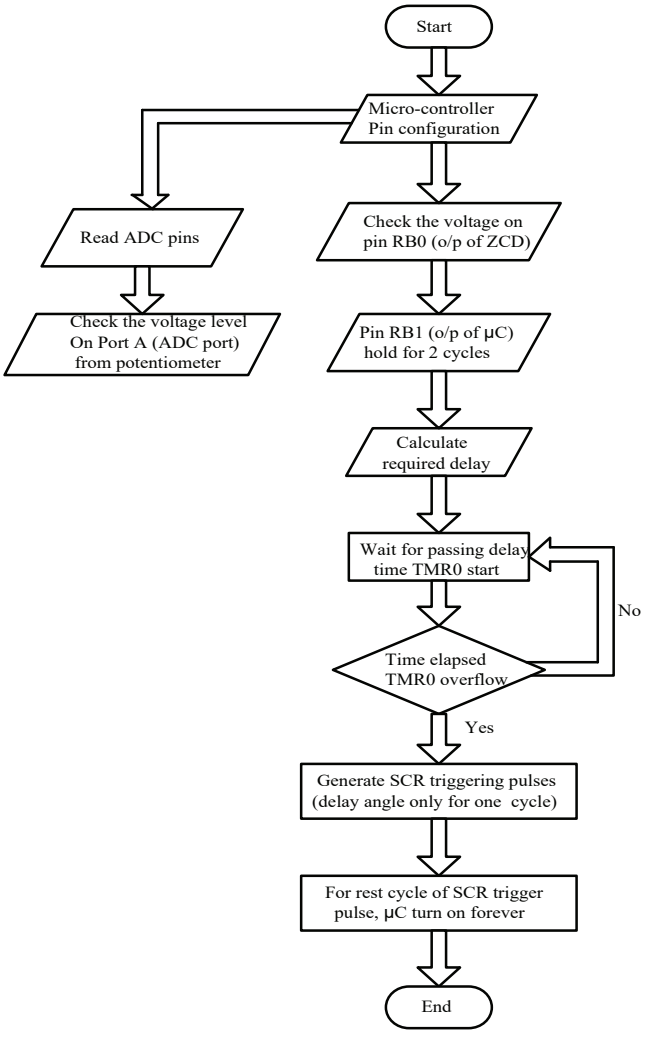


**Figure 9.** Microcontroller programme flow chart. ZCD, zero crossing detector.

ZCD, whose saturation voltage is 15 V, and Ch.C shows the input of the microcontroller, whose amplitude is 4.25 V. Ch.D shows the output of the microcontroller, whose amplitude is 5.25 V with 90° delay angle. The potentiometer varies the delay angle from 0° to 180°. When the potentiometer's position is set as 50%, it corresponds to a delay angle of 90°.

# 5. Experiments with the Set-up

## 5.1. Experiment 1: Study of variation of inrush current with variation in input impedance (for a fixed triggering angle and fixed input voltage)

- The experimental set-up involves a 1 kVA, 50 Hz, 220 V/110 V, shell-type transformer and the appropriate control circuitry. The set-up has been configured for a no-load condition.
- Throughout the experiment, the triggering angle and the input voltage were kept constant. The triggering angle has been set at 36° (1 V), while the supply voltage has been maintained at 220 V. Table 5 presents the analog input and its corresponding angle.
- Different input impedances can be connected to the primary side of the transformer by utilizing 11 Ω, 8.5 A-rated rheostat in series configuration.

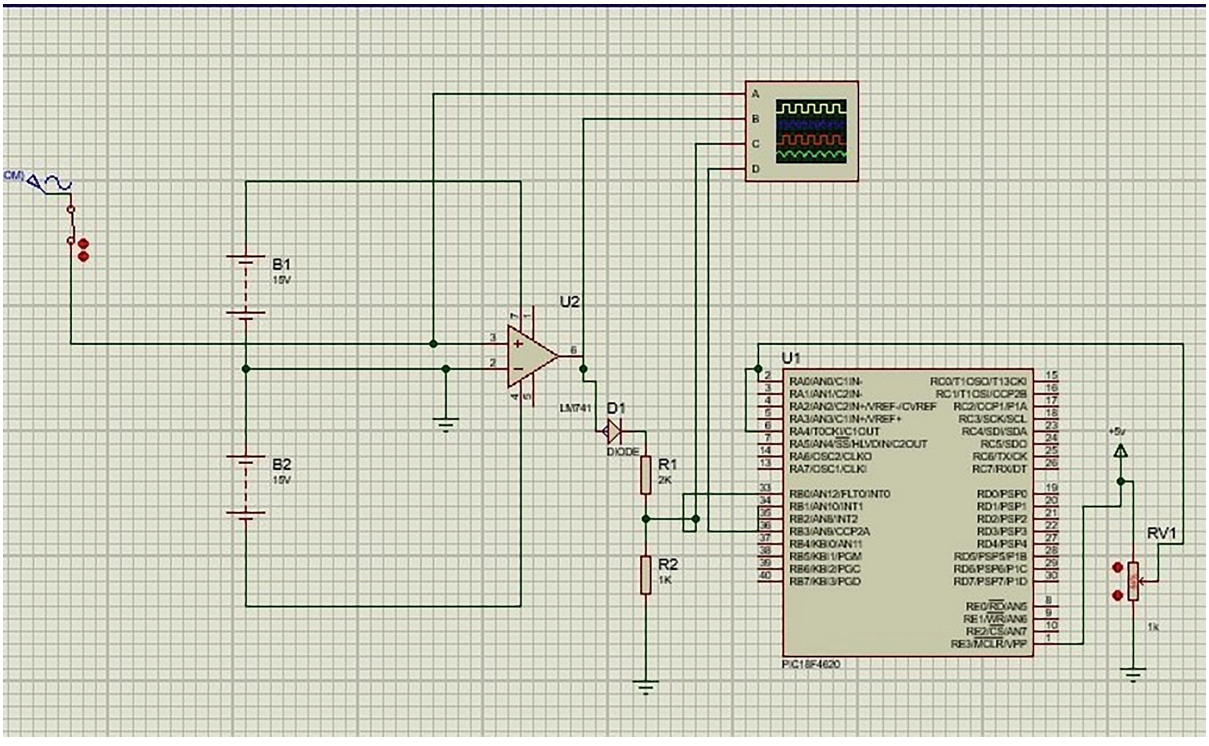


**Figure 10.** Schematic diagram of ZCD and the firing angle of adjustment circuit. ZCD, zero crossing detector.

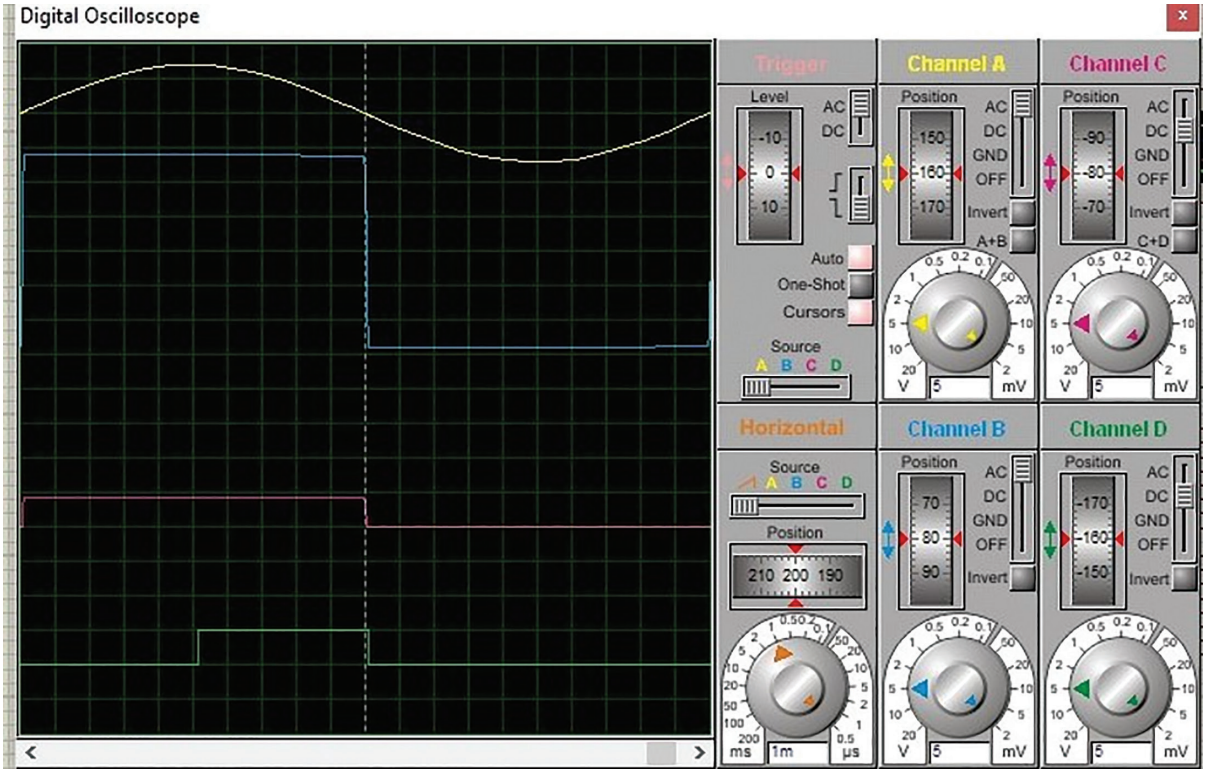


**Figure 11.** Waveforms at different points of Figure 10. Ch.A is supply voltage, Ch.B is o/p of OP-AMP, Ch.C is i/p of microcontroller, and Ch.D is o/p of microcontroller. Scales: X-axis: 1 ms/div, Y-axis: 5 V/div (for Ch. A, B, C, and D).

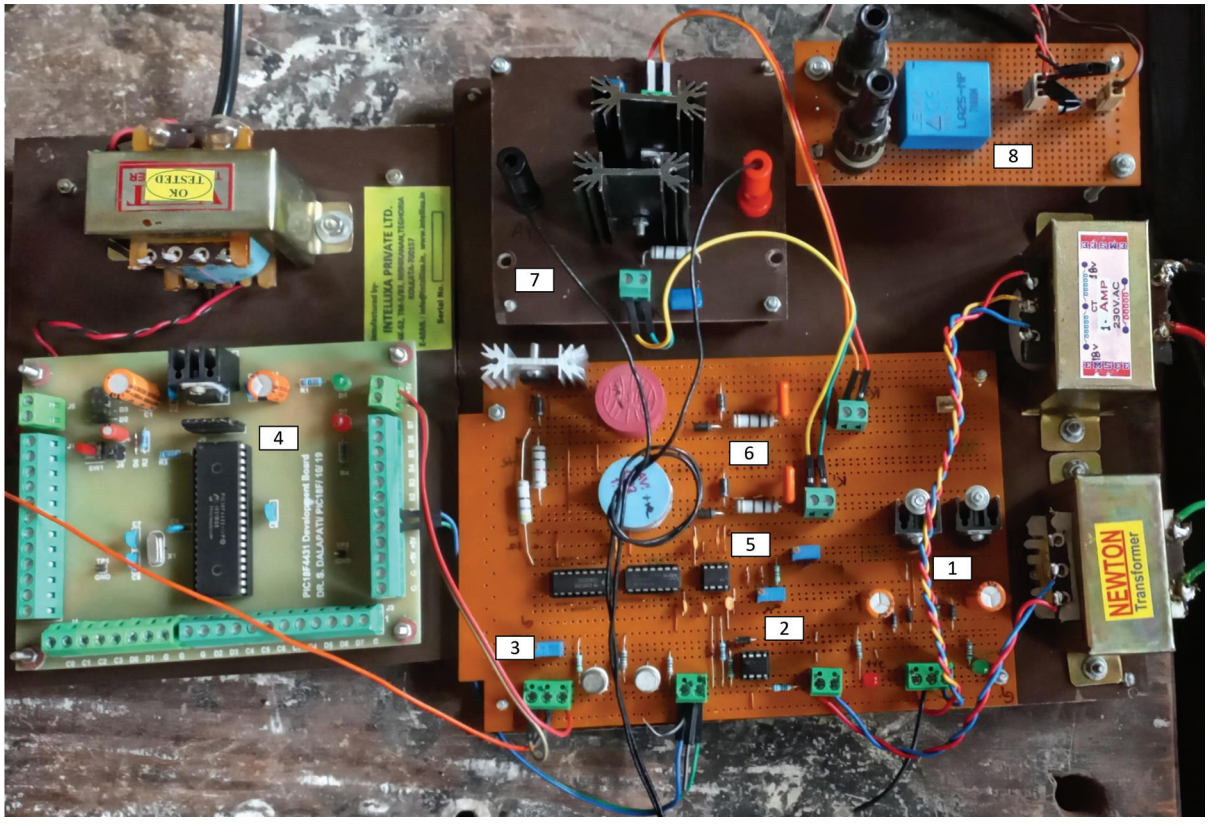


**Figure 12.** Experimental set-up of triggering SCR: 1: power supply circuit 2: ZCD circuit 3: potentiometer for firing angle 4: PIC18F4620 Microcontroller board 5: Timer circuit 6: Driver circuit7: Anti-parallel Thyristor pair 8: Current Sensor. ZCD, zero crossing detector.

- The inrush current has been measured and recorded for each input impedance value using a DSO.
- The measurements have been repeated for multiple input impedance values.

The experimental set-up is shown in Figures 12 and 13. Table 6 presents the variation of the inrush current with change in input impedance, while maintaining a fixed triggering angle and input voltage, and Figure 14 shows the variation in peak-to-peak deflection of the first cycle of inrush current with change in input impedance. It is observed that as the input impedance decreases, both the peak value of the inrush current and the settling time increase. The settling time is determined based on significant changes in the current value, but it should be noted that there may be some transient dips present for a few cycles following the settling value. Figure 15 shows the waveform of inrush current at a 220 V supply voltage, 6 Ω input impedance, and 36° triggering angle.

## 5.2. Experiment 2: Study of variation of inrush current with variation in firing angle (for a fixed input voltage and input impedance)

- The experimental set-up described earlier has been modified, with the transformer, thyristor, and appropriate control circuitry.
- Throughout the experiment, the input voltage and input impedance have been kept constant. No external impedance has been connected to the primary winding of the transformer, and the supply voltage has been maintained at 220 V.
- The firing angle of the thyristor has been varied by adjusting the potentiometer.
- The inrush current has been measured for each firing angle by using a DSO.

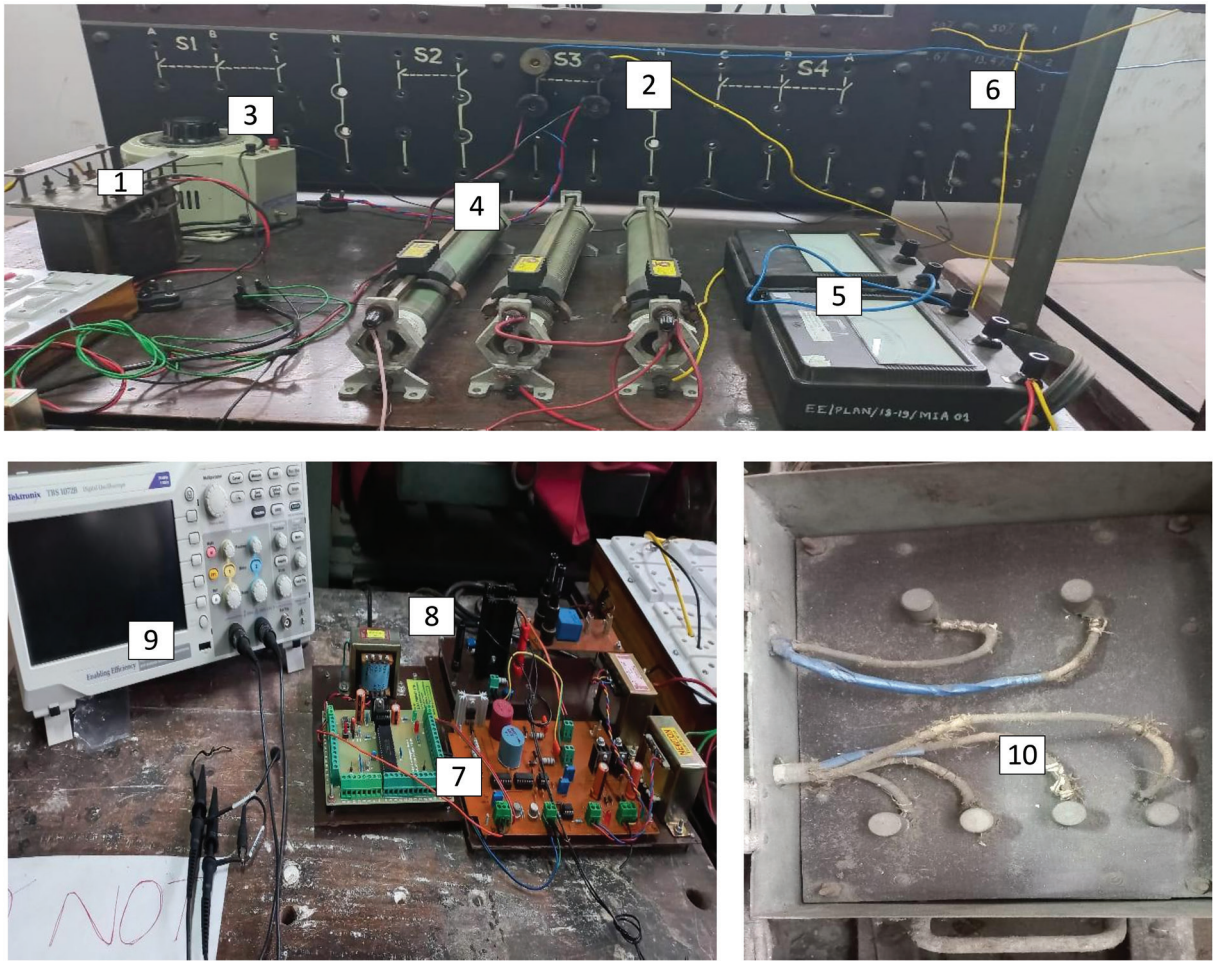


**Figure 13.** Complete hardware set-up: 1: Isolation transformer for DSO, 2: Main supply switching board, 3: Variac, 4: External resistance, 5: Ammeter, 6: Transformer connected board, 7: Control circuit board, 8: Anti-parallel thyristor connected board, 9: DSO, 10: Single-phase, 1 kVA, 50 Hz, 1:1, shell-type transformer. DSO, digital storage oscilloscope.

Table 7 presents the variation of the inrush current with change in firing angle, while maintaining a fixed input voltage and input impedance, and Figure 16 shows the variation in peak-to peak-deflection of the first cycle of inrush current with change in firing angle. A 5 kΩ potentiometer has been used to adjust the firing angle of the thyristor. The potentiometer has been supplied with 5 V DC and adjusted from 0° to 180°. In this potentiometer, 5 V represents 180° and 1 V represents 36°. It has been observed that when the firing angle of the thyristor decreases, both the peak point of the inrush current and the settling time increase. The settling time is determined based on significant change in the current value, but it should be noted that there may be some transient dips present for a few cycles following the settling value. Figure 17 shows the waveform of inrush current at a 220 V supply voltage, and 90° firing angle without any input impedance.

## 5.3. Experiment 3: Study of variation of inrush current with variation in input voltage (for fixed firing angle and input impedance)

- Throughout the experiment, the input impedance and the firing angle have been kept constant. No external impedance is connected to the primary side winding of the transformer, and the triggering angle was set at 90° (2.5 V).

**Table 6.** Study of variation of inrush current with variation in input impedance.

| Sl. No. | Primary side external resistance (Ω) | Current reading taken from DSO (A) | | Time to settle (cycle) |
|---|---|---|---|---|
| | | Peak point of current | Steady state current | |
| 1 | 12 | 5.2 | 1.4 | 4 |
| 2 | | 4.6 | | 3 |
| 3 | | 4.2 | | 3 |
| 4 | | 5 | | 3 |
| 5 | 11 | 7.3 | 1.4 | 4 |
| 6 | | 6.4 | | 3 |
| 7 | | 6 | | 3 |
| 8 | | 6.8 | | 4 |
| 9 | 9 | 7.6 | 1.4 | 3 |
| 10 | | 8 | | 3 |
| 11 | | 13.2 | | 4 |
| 12 | | 9.4 | | 4 |
| 13 | 7 | 10.5 | 1.4 | 4 |
| 14 | | 12 | | 5 |
| 15 | | 10.8 | | 5 |
| 16 | | 11.2 | | 4 |
| 17 | 6 | 10 | 1.4 | 5 |
| 18 | | 18 | | 6 |
| 19 | | 15 | | 5 |
| 20 | | 12.6 | | 5 |
| 21 | 4 | 16 | 1.4 | 7 |
| 22 | | 18.4 | | 8 |
| 23 | | 17.6 | | 7 |
| 24 | | 16.8 | | 7 |
| 25 | 3 | 18.8 | 1.4 | 9 |
| 26 | | 19.4 | | 10 |
| 27 | | 20 | | 10 |
| 28 | | 16.8 | | 9 |
| 29 | 1 | 22.6 | 1.4 | 12 |
| 30 | | 25 | | 13 |
| 31 | | 26.2 | | 13 |
| 32 | | 27.3 | | 13 |

DSO, digital storage oscilloscope.

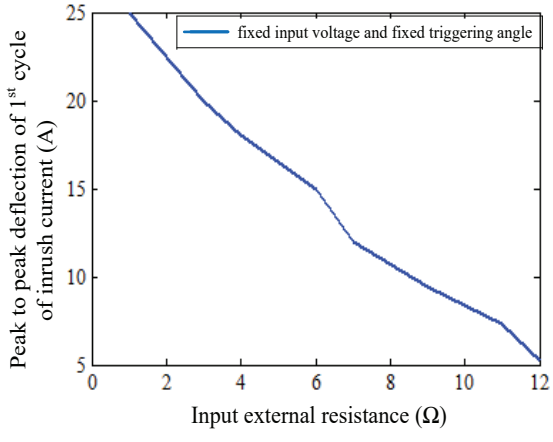


**Figure 14.** Peak-to-peak deflection of the first cycle of inrush current with variation in input impedance (for a fixed triggering angle and fixed input voltage); Scales: X-axis: 2 Ω/div Y-axis: 5 A/div.

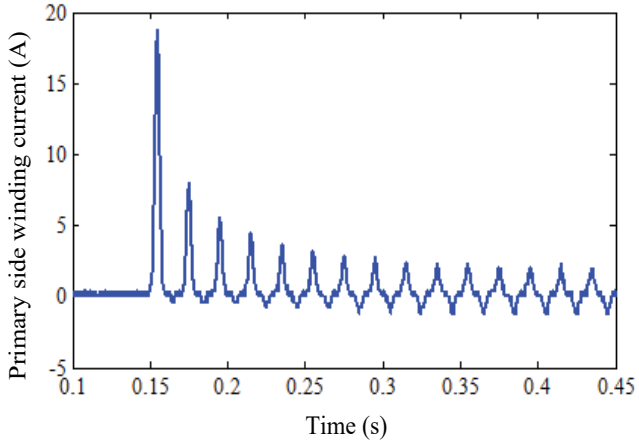


**Figure 15.** Waveform of primary side winding current at a 220 V supply voltage, 6 Ω input impedance, and 36° triggering angle. Scales: X-axis: 50 ms/div; Y-axis: 5 A/div.

**Table 7.** Study of variation of inrush current with variation in firing angle.

| Sl. No. | Firing angle (°) | Current reading taken from DSO (A) | | Time to settle (cycle) |
|---|---|---|---|---|
| | | Peak point of current | Steady state current | |
| 1 | 90 | 4.1 | 1.4 | 7 |
| 2 | | 5.6 | | 8 |
| 3 | | 6 | | 7 |
| 4 | | 4.3 | | 7 |
| 5 | 72 | 18 | 1.4 | 8 |
| 6 | | 19 | | 8 |
| 7 | | 20 | | 8 |
| 8 | | 10 | | 8 |
| 9 | 54 | 28.6 | 1.4 | 9 |
| 10 | | 32.4 | | 9 |
| 11 | | 30 | | 9 |
| 12 | | 29 | | 9 |
| 13 | 36 | 44.8 | 1.4 | 10 |
| 14 | | 40.4 | | 10 |
| 15 | | 44.8 | | 10 |
| 16 | | 38 | | 10 |
| 17 | 18 | 40.8 | 1.4 | 10 |
| 18 | | 45.5 | | 11 |
| 19 | | 44.6 | | 10 |
| 20 | | 45 | | 10 |
| 21 | 0 | 45 | 1.4 | 11 |
| 22 | | 46 | | 11 |
| 23 | | 42 | | 11 |
| 24 | | 45.5 | | 11 |

DSO, digital storage oscilloscope.

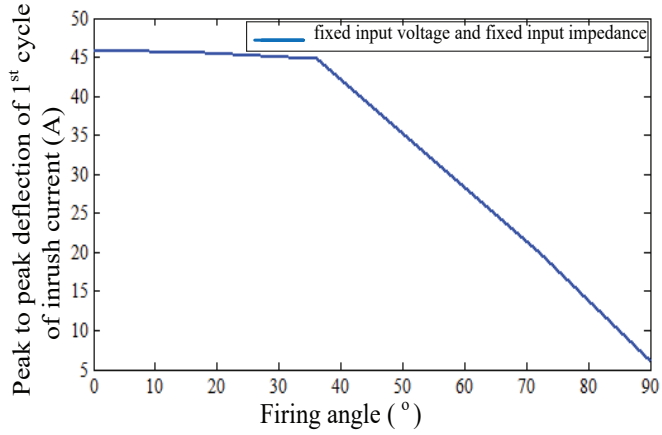


**Figure 16.** Variation of inrush current with variation in firing angle (for a fixed input voltage and fixed input impedance) Scales: X-axis: 10°/div; Y-axis: 5 A/div.

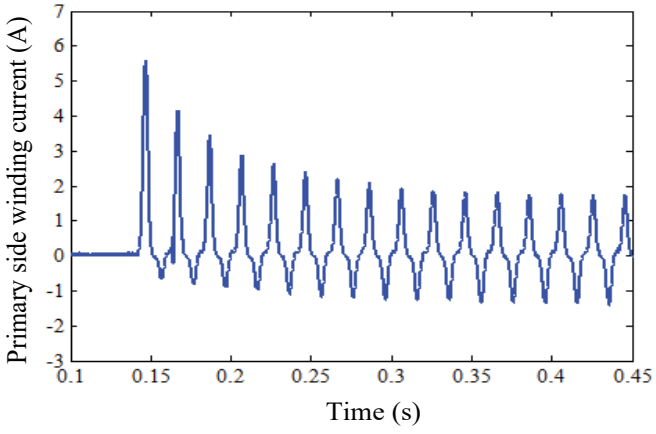


**Figure 17.** Waveform of primary side winding current at a 220 V supply voltage, no input impedance, and 90° triggering angle. Scales: X-axis: 50 ms/div; Y-axis: 1 A/div.

- The input voltage supplied to the primary side of the transformer has been varied by adjusting the 240 V/0–240–270 V, 4 A, 50 Hz variac.
- The inrush current is recorded for each input voltage level using DSO.

Table 8 presents the variation of the inrush current with change in input voltage, while maintaining a fixed firing angle and input impedance, and Figure 18 shows the variation in peak-to-peak deflection of the first cycle of the inrush current with changes in input voltage. It is observed that when the input voltage increases, both the peak point of the inrush current and the steady state current increase. The experiments have been conducted to study the variation of the inrush current with respect to the input impedance, firing angle, and input voltage, as well as the settling time of inrush current, in different cases. The analysis of the data has revealed important conclusions. Firstly, the inrush current is found to vary with change in input impedance, indicating an indirect relationship between the two. Secondly, there is a clear correlation between the firing angle and the inrush current, where lower firing angles result in larger inrush currents. Thirdly, the input voltage is observed to affect the magnitude of the inrush current, demonstrating a direct impact on it. Lastly, the experiments show that the settling time of the inrush current increases with lower input impedance, suggesting that it takes a longer time for the current to stabilize when the input impedance is low.

**Table 8.** Study of variation of inrush current with variation in input voltage.

| Sl. No. | Supply voltage (V) | Current reading taken from DSO (A) | | Time to settle (cycle) |
|---|---|---|---|---|
| | | Peak point of current | Steady state current | |
| 1 | 80 | 0.2 | 0.1 | 6 |
| 2 | | 0.4 | | 6 |
| 3 | | 0.28 | | 6 |
| 4 | | 0.36 | | 6 |
| 5 | 100 | 0.5 | 0.2 | 7 |
| 6 | | 0.75 | | 8 |
| 7 | | 0.45 | | 7 |
| 8 | | 0.6 | | 7 |
| 9 | 130 | 1.4 | 0.37 | 7 |
| 10 | | 1.3 | | 7 |
| 11 | | 1 | | 7 |
| 12 | | 1.35 | | 7 |
| 13 | 150 | 2 | 0.5 | 8 |
| 14 | | 1.8 | | 7 |
| 15 | | 1.5 | | 7 |
| 16 | | 1.9 | | 8 |
| 17 | 170 | 2.1 | 0.8 | 7 |
| 18 | | 2.3 | | 8 |
| 19 | | 1.7 | | 7 |
| 20 | | 1.9 | | 7 |
| 21 | 180 | 1.8 | 1 | 7 |
| 22 | | 2.5 | | 7 |
| 23 | | 2 | | 7 |
| 24 | | 1.7 | | 7 |
| 25 | 200 | 4 | 1.24 | 7 |
| 26 | | 3.3 | | 7 |
| 27 | | 3.8 | | 7 |
| 28 | | 4 | | 7 |
| 29 | 220 | 4.1 | 1.5 | 7 |
| 30 | | 5.6 | | 8 |
| 31 | | 6 | | 8 |
| 32 | | 4.3 | | 7 |

DSO, digital storage oscilloscope.

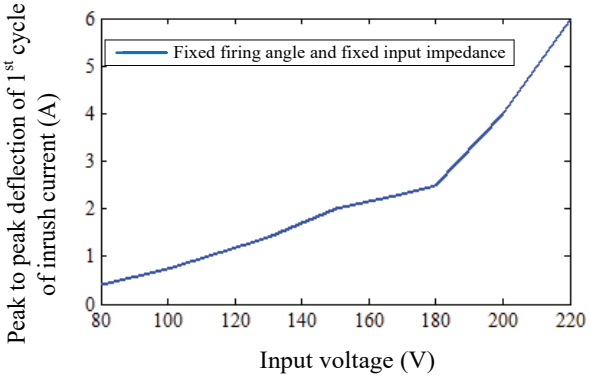


**Figure 18.** Variation of inrush current with variation in input voltage (for a fixed input impedance and fixed firing angle); Scales: X-axis: 20 V/div; Y-axis: 1 A/div.

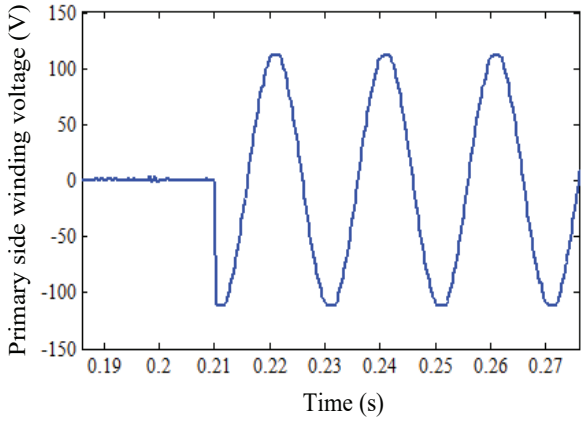


**Figure 19.** Waveform of transformer primary side impressed voltage at 72°; Scales: X-axis: 10 ms/div; Y-axis: 50 V/div.

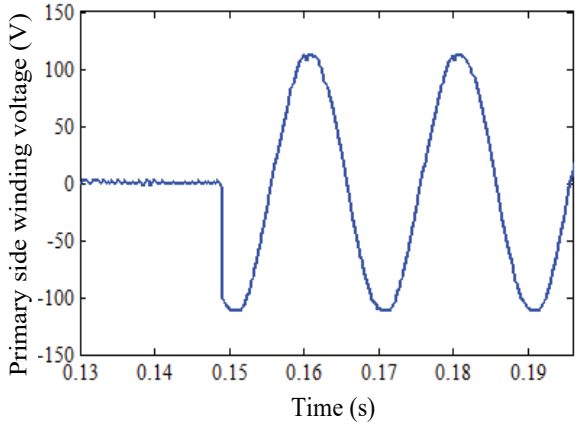


**Figure 20.** Waveform of transformer primary side impressed voltage at 54°; Scales: X-axis: 10 ms/div; Y-axis: 50 V/div.

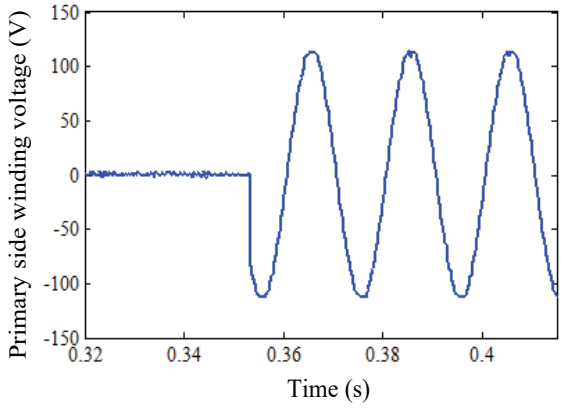


**Figure 21.** Waveform of transformer primary side impressed voltage at 36°; Scales: X-axis: 20 ms/div; Y-axis: 50 V/div.

These findings highlight the importance of considering input impedance, firing angle, and input voltage in managing inrush current, and providing useful information for designing and optimizing systems to mitigate inrush current-related issues. Figures 19–21 show the transformer primary side impressed voltage waveform at 80 V supply voltage and different firing angles.

# 6. Conclusion

Continuous research is going on for analysing the MIC and its effects on the system, which helped in developing new techniques for reducing it. Some of the techniques have been developed for discriminating the inrush current from the internal fault current, whereas some others involve the asynchronous closing technology-based strategy, controlled switching strategy, and modified time difference technique. Recent developments in this area involve the wavelet transform, particle swarm algorithm-based optimized support vector machine (SVM), empirical mode decomposition etc.

The present manuscript has been written from a completely different point of view. Generally in under-graduate studies, theoretical discussion is included regarding MIC without giving much practical exposure. This paper actually presents the development of a low-cost experimental set-up using a digital controller to study the MIC phenomenon and the different parameters which can affect the same. This also helps in showing how the inrush current can be minimised. This set-up provides a direct hands-on experience with MIC and its control in under-graduate study, which can help an upcoming practitioner in industry as well as in further research.

The major contribution of this paper is the making of an experimental set-up for analysing and reducing the transformer inrush current by the point-on-wave method, and involves the design and implementation of a control circuit. The circuit incorporates components such as a zero-crossing detector, microcontroller, signal amplifier, driver circuit, and isolation circuit. The zero-crossing detector synchronises the operation of the thyristor with the AC supply voltage, while the microcontroller processes the signal to determine the desired timing and delay for thyristor triggering. The signal amplifier amplifies the control signal, which is then fed into the driver circuit to provide the necessary gate voltage and current pulses to trigger the thyristor. An isolation circuit is also included to protect the control circuitry from electrical noise and potential hazards. Through systematic experimentation and optimization, the set-up has successfully reduced the inrush current of the transformer by precisely controlling the thyristor's triggering.

In conclusion, this paper demonstrates the effectiveness of the point-on-wave method for reducing the transformer inrush current. By implementing the experimental set-up and control circuit, this work has successfully achieved the desired target of minimising the inrush current during transformer energisation. The use of a precise triggering mechanism through the integration of a low-cost digital controller allows the accurate control over the thyristor's operation. The experimental results confirm the success of developing the experimental set-up for checking the feasibility and practicality of the point-on-wave method as a means to mitigate inrush current, thereby enhancing the efficiency and reliability of transformer operations.

## References


Al-Khalifah, A. K. and El Saadany, E. F. (2006). Investigation of magnetizing inrush current in a single-phase transformer. In: *Proceedings of the IEEE Large Engineering Systems Conference on Power Engineering*, 26-28 July, 2006, Halifax, NS, Canada, pp. 165–171.

Avinash, L. R. (2015). Repression of Transformer Inrush Current. In: *IJCA Proceedings of National Conference on Power Systems and Industrial Automation*, NCPSIA 2015(2), 27-30 December, 2015, pp. 4–6.

Basu, K. P. and Asghar, A. (2008). Reduction of magnetising inrush current in a delta- connected transformer. In: *Proceedings of the IEEE 2nd International Power and Energy Conference*, 1-3 December, 2008, Johor Bahru, Malaysia, pp. 35–38.

Batista, Y. N., Souza, H. E. P. D., Neves, F. D. A. D. S., and Filho, R. F. D. (2018). A GDSC-based Technique to Distinguish Transformer Magnetising from Fault Currents. *IEEE Transactions on Power Delivery*, 33(2), pp. 110–118. doi: 10.1109/TPWRD.2017.2691670.

Bi, D. Q., Zhang, X. A., Yang, H. H., Yu, G. W., Wang, X. H., and Wang, W. J. (2007). Correlation Analysis of Waveforms in Non-saturation Zone-based Method to Identify the Magnetizing Inrush in Transformer. *IEEE Transactions on Power Delivery*, 22(3), pp.1380–1385.doi:10.1109/TPWRD.2007.900147.

Bimbhra, P. S. (2007). *Generalised Theory of Electrical Machines*, 5th ed. India: Khanna Publishers, pp. 967–980.

Blume, L. F., Camilli, G., Farnham, S. B., and Peterson, H. A. (1944). Transformer Magnetizing Inrush

Currents and Influence on System Operation. *Transactions of the American Institute of Electrical Engineers (AIEE)*, 63(6), pp. 366–375. doi: 10.1109/T-AIEE.1944.5058946.

Chen, Z., Li, H., Dong, X., He, Y., Zhou, Q., Zhang, Y., and Zhang, Y. (2023). Magnetizing Inrush Current Elimination Strategy Based on a Parallel-type Asynchronous Closing Hybrid Transformer. *IEEE Transactions on Power Electronics*, 38(1), pp. 931–943. doi: 10.1109/TPEL.2022.3196229.

Duan, P., Yang, Z., He, Y., Zhang, B., Zhang, L., Liu, F., and Shi, Y. (2022). Research on Identification of Magnetizing Inrush Current Based on PSO-SVM. In: *Proceedings of the 4th Asia Energy and Electrical Engineering Symposium*, 25-28 March, 2022, Chengdu, China, pp. 630–634.

Faiz, J. and Lotfi-Fard, S. (2006). A Novel Wavelet-based Algorithm for Discrimination of Internal Faults from Magnetizing Inrush Currents in Power Transformers. *IEEE Transactions on Power Delivery*, 22(3), pp. 1989–1996. doi: 10.1109/TPWRD.2006.877095.

Farazmand, A., León, F. D., Zhang, K., and Jazebi, S. (2014). Analysis, Modeling, and Simulation of the Phase-Hop Condition in Transformers: The Largest Inrush Currents. *IEEE Transactions on Power Delivery*, 29(4), pp. 1918–1926. doi: 10.1109/TPWRD.2013.2286828.

Hamilton, R. (2013). Analysis of Transformer Inrush Current and Comparison of Harmonic Restraint Methods in Transformer Protection. *IEEE Transactions on Industry Applications*, 49(4), pp. 1890–1899. doi: 10.1109/TIA.2013.2257155.

He, B., Zhang, X., and Bo, Z. Q. (2006). A New Method to Identify Inrush Current Based on Error Estimation. *IEEE Transactions on Power Delivery*, 21(3), pp. 1163–1168. doi: 10.1109/TPWRD.2005.861337.

Hooshyar, A., Sanaye-Pasand, M., Afsharnia, S., Davarpanah, M., and Ebrahimi, B. M. (2012). Time-Domain Analysis of Differential Power Signal to Detect Magnetizing Inrush in Power Transformers. *IEEE Transactions on Power Delivery*, 27(3), pp. 1394–1404. doi: 10.1109/TPWRD.2012.2197869.

Jamali, M., Mirzaie, M., and Gholamian, S. (2011). Calculation and Analysis of Transformer Inrush Current Based on Parameters of Transformer and Operating Conditions. *Electronics and Electrical Engineering*, 109, pp. 1392–1215. doi: 10.5755/j01.eee.109.3.162.

Jazebi, S., León, F. D., and Wu, N. (2015). Enhanced Analytical Method for the Calculation of the Maximum Inrush Currents of Single-Phase Power Transformers. *IEEE Transactions on Power Delivery*, 30(6), pp. 2590–2599. doi: 10.1109/TPWRD.2015.2443560.

Jin, N., Xing, J., Lin, X., Zhang, P., Rong, Z., Tong, Z., and Li, Z. (2020). Countermeasure on Preventing Line Zero-Sequence Overcurrent Protection from Mal-Operation due to Magnetizing Inrush. *IEEE Transactions on Power Delivery*, 35(3), pp. 1476–1487. doi: 10.1109/TPWRD.2019.2946641.

Kumar. P. and Reddy. S. Y. (2014). Optimisation of Inrush Current in Electrical Transformer. In: *Proceedings of the International Conference on Smart Electric Grid (ISEG)*, 19-20 September, 2014, Guntur, India, pp. 1–5.

León, F. D., Farazmand, A., and Joseph, P. (2012). Comparing the T and Equivalent Circuits for the Calculation of Transformer Inrush Currents. *IEEE Transactions on Power Delivery*, 27(4), pp. 2390–2398. doi: 10.1109/TPWRD.2012.2208229.

Liu, Z., Xiao, S. and Dong, S. (2021). Identification of Transformer Magnetizing Inrush Current Based on Empirical Mode Decomposition, In: *Proceedings of the IEEE 4th Electrical and Energy Conference (CIEEC)*, 28-30 May,2021, Wuhan, China, pp. 1–6.

Medeiros, R. P. and Costa, F. B. (2018). A Wavelet-based Transformer Differential Protection: Internal Fault Detection during Inrush Conditions. *IEEE Transactions on Power Delivery*, 33(6), pp. 2965–2977. doi: 10.1109/TPWRD.2018.2852485.

Mirkalaei, S. A. M. and Hashiesh, F. (2015). Controlled Switching to Mitigate Power Transformers Inrush Current Phenomenon. In: *Proceedings of the 50th International Universities Power Engineering Conference (UPEC)*, 1-4 September, 2015, Stoke on Trent, UK, pp. 1–4.

Mohan, N., Undeland, T., and Robbins, W. (2003). *Power Electronics: Converters, Applications, and Design*. John Wiley & Sons, Sahibabad, India

Moreira, R. F. P., Cleff, V. M., Souza, E. G., and Nascimento, C. D. D. (2021). Gradient-based algorithm for the Distinction of Fault and Inrush Currents in Low Power Transformers. In: *Proceedings of the IEEE URUCON*. 24-26 November, 2021, Montevideo, Uruguay, pp. 467–471.

Naseri, F., Kazemi, Z., Arefi, M. M. and Farjah, E. (2018). Countermeasure on Preventing Line Zero-Sequence Overcurrent Protection from Mal-Operation due to Magnetizing Inrush. *IEEE Transactions on Power Delivery*, 33(1), pp. 110–118. doi: 10.1109/TPWRD.2017.2695568.

Negara, Y., Darmawan, D. W., Nurdianto, R., Riawan, D. C., and Musthofa, A. (2017). Demagnetization Method for Reducing Inrush Current of Single Phase 1kVA Transformer. *Journal on Advance Research in Electrical Engineering (JAREE)*. April 2017, Volume 1, Number 1, pp. 55–61.

Pachore, P., Gupta, Y., Anand, S., Sarkar, S., Mathur, P., and Singh, P. K. (2021). Flux Error Function-based Controlled Switching Method for Minimizing Inrush Current in 3-Phase Transformer. *IEEE Transactions on Power Delivery*, 36(2), pp. 870–879. doi: 10.1109/TPWRD.2020.2995519.

Sobrinho, A. M., Camacho, J. R., Malagoli, J. A., and Mamede, A. C. F. (2016). Analysis of the Maximum Inrush Current in the Optimal Design of a Single Phase Transformer. *IEEE Latin America Transactions*, 14(12), pp. 4706–4714. doi: 10.1109/TLA.2016.7817001.

Taylor, D. I., Law, J. D., Johnson, B. K. and Fischer, N. (2012). Single-Phase Transformer Inrush Current Reduction using Prefluxing. *IEEE Transactions on Power Delivery*, 27(1), pp. 245–252. doi: 10.1109/TPWRD.2011.2174162.

Wang, E., Bai, J. and Liu, H. (2023). Research On Magnetizing Inrush Current and Fault Identification of Transformer Based on Wavelet Analysis. In: *Proceedings of the IEEE 5th International Conference on Civil Aviation Safety and Information Technology (ICCASIT)*, 11-13 October, 2023, Dali, China, pp. 1010–1013.

Wani, M., Kurundkar, K. and Bhawalkar, M. P. (2012). Use of Power Electronic Converters to Suppress Transformer Inrush Current. In: *Proceedings of the IEEE International Conference on Power Electronics, Drives and Energy Systems (PEDES)*, 16-19 December, 2012, Bengaluru, India, pp. 1–5.

Yahiou, A., Adi, A. B., Mellah, H., Abid, M., R'Gueyeg, M. S. and Merabet, A. O. (2022). Inrush Current Influence on the Hysteresis Loop of a Single-Phase Transformer. In: *Proceedings of the 19th International Multi- Conference on Systems, Signals & Devices (SSD)*, 6-10 May, 2022, Sétif, Algeria, pp. 18171–18179.